Combined Analysis of ν_μ Disappearance and $\nu_\mu \rightarrow \nu_e$ Appearance in MINOS Using Accelerator and Atmospheric Neutrinos

P. Adamson,[8] I. Anghel,[15,1] A. Aurisano,[7] G. Barr,[21] M. Bishai,[3] A. Blake,[5] G. J. Bock,[8] D. Bogert,[8] S. V. Cao,[29]
C. M. Castromonte,[9] D. Cherdack,[30] S. Childress,[8] J. A. B. Coelho,[30,6] L. Corwin,[14] D. Cronin-Hennessy,[18] J. K. de Jong,[21]
A. V. Devan,[32] N. E. Devenish,[27] M. V. Diwan,[3] C. O. Escobar,[6] J. J. Evans,[17] E. Falk,[27] G. J. Feldman,[10] M. V. Frohne,[11]
H. R. Gallagher,[30] R. A. Gomes,[9] M. C. Goodman,[1] P. Gouffon,[24] N. Graf,[22,13] R. Gran,[19] K. Grzelak,[31] A. Habig,[19]
S. R. Hahn,[8] J. Hartnell,[27] R. Hatcher,[8] A. Himmel,[4] A. Holin,[16] J. Huang,[29] J. Hylen,[8] G. M. Irwin,[26] Z. Isvan,[3,22]
C. James,[8] D. Jensen,[8] T. Kafka,[30] S. M. S. Kasahara,[18] G. Koizumi,[8] M. Kordosky,[32] A. Kreymer,[8] K. Lang,[29] J. Ling,[3]
P. J. Litchfield,[18,23] P. Lucas,[8] W. A. Mann,[30] M. L. Marshak,[18] N. Mayer,[30,14] C. McGivern,[22] M. M. Medeiros,[9]
R. Mehdiyev,[29] J. R. Meier,[18] M. D. Messier,[14] D. G. Michael,[4,*] W. H. Miller,[18] S. R. Mishra,[25] S. Moed Sher,[8]
C. D. Moore,[8] L. Mualem,[4] J. Musser,[14] D. Naples,[22] J. K. Nelson,[32] H. B. Newman,[4] R. J. Nichol,[16] J. A. Nowak,[18]
J. O'Connor,[16] M. Orchanian,[4] R. B. Pahlka,[8] J. Paley,[1] R. B. Patterson,[4] G. Pawloski,[18,26] A. Perch,[16] S. Phan-Budd,[1]
R. K. Plunkett,[8] N. Poonthottathil,[8] X. Qiu,[26] A. Radovic,[32,16] B. Rebel,[8] C. Rosenfeld,[25] H. A. Rubin,[13] M. C. Sanchez,[15,1]
J. Schneps,[30] A. Schreckenberger,[29,18] P. Schreiner,[1] R. Sharma,[8] A. Sousa,[7,10] N. Tagg,[20] R. L. Talaga,[1] J. Thomas,[16]
M. A. Thomson,[5] X. Tian,[25] A. Timmons,[17] S. C. Tognini,[9] R. Toner,[10,5] D. Torretta,[8] G. Tzanakos,[2] J. Urheim,[14] P. Vahle,[32]
B. Viren,[3] A. Weber,[21,23] R. C. Webb,[28] C. White,[13] L. Whitehead,[12,3] L. H. Whitehead,[16] S. G. Wojcicki,[26] and R. Zwaska[8]

(MINOS Collaboration)

[1]*Argonne National Laboratory, Argonne, Illinois 60439, USA*
[2]*Department of Physics, University of Athens, GR-15771 Athens, Greece*
[3]*Brookhaven National Laboratory, Upton, New York 11973, USA*
[4]*Lauritsen Laboratory, California Institute of Technology, Pasadena, California 91125, USA*
[5]*Cavendish Laboratory, University of Cambridge, Madingley Road, Cambridge CB3 0HE, United Kingdom*
[6]*Universidade Estadual de Campinas, IFGW-UNICAMP, CP 6165, 13083-970 Campinas, SP, Brazil*
[7]*Department of Physics, University of Cincinnati, Cincinnati, Ohio 45221, USA*
[8]*Fermi National Accelerator Laboratory, Batavia, Illinois 60510, USA*
[9]*Instituto de Física, Universidade Federal de Goiás, CP 131, 74001-970 Goiânia, GO, Brazil*
[10]*Department of Physics, Harvard University, Cambridge, Massachusetts 02138, USA*
[11]*Holy Cross College, Notre Dame, Indiana 46556, USA*
[12]*Department of Physics, University of Houston, Houston, Texas 77204, USA*
[13]*Department of Physics, Illinois Institute of Technology, Chicago, Illinois 60616, USA*
[14]*Indiana University, Bloomington, Indiana 47405, USA*
[15]*Department of Physics and Astronomy, Iowa State University, Ames, Iowa 50011 USA*
[16]*Department of Physics and Astronomy, University College London, Gower Street, London WC1E 6BT, United Kingdom*
[17]*School of Physics and Astronomy, University of Manchester, Oxford Road, Manchester M13 9PL, United Kingdom*
[18]*University of Minnesota, Minneapolis, Minnesota 55455, USA*
[19]*Department of Physics, University of Minnesota Duluth, Duluth, Minnesota 55812, USA*
[20]*Otterbein College, Westerville, Ohio 43081, USA*
[21]*Subdepartment of Particle Physics, University of Oxford, Oxford OX1 3RH, United Kingdom*
[22]*Department of Physics and Astronomy, University of Pittsburgh, Pittsburgh, Pennsylvania 15260, USA*
[23]*Rutherford Appleton Laboratory, Science and Technologies Facilities Council, Didcot OX11 0QX, United Kingdom*
[24]*Instituto de Física, Universidade de São Paulo, CP 66318, 05315-970 São Paulo, SP, Brazil*
[25]*Department of Physics and Astronomy, University of South Carolina, Columbia, South Carolina 29208, USA*
[26]*Department of Physics, Stanford University, Stanford, California 94305, USA*
[27]*Department of Physics and Astronomy, University of Sussex, Falmer, Brighton BN1 9QH, United Kingdom*
[28]*Physics Department, Texas A&M University, College Station, Texas 77843, USA*
[29]*Department of Physics, University of Texas at Austin, 1 University Station C1600, Austin, Texas 78712, USA*
[30]*Physics Department, Tufts University, Medford, Massachusetts 02155, USA*
[31]*Department of Physics, University of Warsaw, Hoża 69, PL-00-681 Warsaw, Poland*
[32]*Department of Physics, College of William & Mary, Williamsburg, Virginia 23187, USA*

We report on a new analysis of neutrino oscillations in MINOS using the complete set of accelerator and atmospheric data. The analysis combines the ν_μ disappearance and ν_e appearance data using the three-flavor

formalism. We measure $|\Delta m_{32}^2| = [2.28\text{--}2.46] \times 10^{-3}$ eV^2 (68% C.L.) and $\sin^2\theta_{23} = 0.35\text{--}0.65$ (90% C.L.) in the normal hierarchy, and $|\Delta m_{32}^2| = [2.32\text{--}2.53] \times 10^{-3}$ eV^2 (68% C.L.) and $\sin^2\theta_{23} = 0.34\text{--}0.67$ (90% C.L.) in the inverted hierarchy. The data also constrain δ_{CP}, the θ_{23} octant degeneracy and the mass hierarchy; we disfavor 36% (11%) of this three-parameter space at 68% (90%) C.L.

The study of neutrino oscillations has entered a precision era in which the experimental data can be used to probe the three-flavor framework of mixing between the neutrino flavor eigenstates (ν_e, ν_μ, ν_τ) and mass eigenstates (ν_1, ν_2, ν_3). In the standard theory, neutrino mixing is described by the unitary PMNS matrix [1], parametrized by three angles θ_{12}, θ_{23}, θ_{13}, and a phase δ_{CP}. The oscillation probabilities additionally depend on the two mass-squared differences Δm_{32}^2 and Δm_{21}^2, where $\Delta m_{ij}^2 \equiv m_i^2 - m_j^2$. The current generation of experiments has measured all three mixing angles and the mass-squared differences using accelerator, atmospheric, reactor, and solar neutrinos [2]. Most recently, the smallest mixing angle, θ_{13}, has been measured precisely by reactor neutrino experiments [3–5]. However, the picture is not yet complete. The value of δ_{CP}, which determines the level of CP violation in the lepton sector, has not yet been measured. It is also not known whether the neutrino mass hierarchy is normal ($\Delta m_{32}^2 > 0$) or inverted ($\Delta m_{32}^2 < 0$), whether $\sin^2 2\theta_{23}$ is maximal, or if not, whether the mixing angle θ_{23} lies in the lower ($\theta_{23} < \pi/4$) or higher ($\theta_{23} > \pi/4$) octant. These unknowns, which are essential to a complete understanding of neutrino mass and mixing, can be probed by long-baseline neutrino experiments.

The MINOS long-baseline experiment [6] has published measurements of oscillations using accelerator and atmospheric neutrinos and antineutrinos. The oscillations observed by MINOS are driven by the larger mass-squared difference Δm_{32}^2; hence, many features of the data can be described by an effective two-flavor model with a single mass-squared difference Δm^2 and mixing angle θ. In this approximation, the ν_μ and $\bar{\nu}_\mu$ survival probabilities are

$$P(\nu_\mu \to \nu_\mu) \approx 1 - \sin^2 2\theta \, \sin^2\left(\frac{\Delta m^2 L_\nu}{4E_\nu}\right), \quad (1)$$

where L_ν is the neutrino propagation distance and E_ν is the neutrino energy. A previous two-flavor analysis of ν_μ and $\bar{\nu}_\mu$ disappearance using the combined accelerator and atmospheric data from MINOS yielded $|\Delta m^2| = 2.41^{+0.09}_{-0.10} \times 10^{-3}$ eV^2 and $\sin^2 2\theta = 0.950^{+0.035}_{-0.036}$ [7]. The statistical weight of the data now enables MINOS to constrain the full three-flavor model of ν_μ and $\bar{\nu}_\mu$ disappearance. The uncertainty on Δm^2 is approaching the size of the smaller mass-squared difference, Δm_{21}^2, which is neglected in the two-flavor model. Moreover, the precise knowledge of θ_{13} enables an analysis of the data based on the full set of mixing parameters. In this Letter we present the three-flavor analysis of the combined MINOS data.

In the three-flavor framework, the oscillations are driven by two mass-squared differences Δm_{32}^2 and Δm_{31}^2, where $\Delta m_{31}^2 = \Delta m_{32}^2 + \Delta m_{21}^2$. The interference between the resulting two oscillation frequencies leads to terms in the oscillation probabilities that depend on all the mixing parameters. The leading-order ν_μ and $\bar{\nu}_\mu$ survival probabilities in vacuum take the same form as the two-flavor approximation in Eq. (1), with the effective parameters given by [8]:

$$\sin^2 2\theta = 4\sin^2\theta_{23}\cos^2\theta_{13}(1 - \sin^2\theta_{23}\cos^2\theta_{13}),$$
$$\Delta m^2 = \Delta m_{32}^2 + \Delta m_{21}^2 \sin^2\theta_{12}$$
$$+ \Delta m_{21}^2 \cos\delta_{CP} \sin\theta_{13} \tan\theta_{23} \sin 2\theta_{12}. \quad (2)$$

The exact symmetries of the two-flavor model under $\theta \to \pi/2 - \theta$ and $\Delta m^2 \to -\Delta m^2$ lead to approximate degeneracies in the octant of θ_{23} and mass hierarchy in the three-flavor formalism.

For neutrinos traveling through matter, the propagation eigenstates are modified by the MSW effect [9]. In this case, the mixing angle θ_{13} is replaced by a modified version, θ_M, given by [10]

$$\sin^2 2\theta_M = \frac{\sin^2 2\theta_{13}}{\sin^2 2\theta_{13} + (A - \cos 2\theta_{13})^2}. \quad (3)$$

The size of the matter effect is determined by the parameter $A \equiv \pm 2\sqrt{2} G_F n_e E_\nu / \Delta m_{31}^2$, where G_F is the Fermi weak coupling constant, n_e is the density of electrons, and the sign of A is positive (negative) for neutrinos (antineutrinos). Equation (3) shows that $\sin^2 2\theta_M$ is maximal at $A = \cos 2\theta_{13}$. This condition leads to the resonant enhancement of $\nu_\mu \leftrightarrow \nu_e$ oscillations, which can significantly alter the magnitude of ν_μ disappearance. The effect is present for neutrinos in the normal hierarchy and for antineutrinos in the inverted hierarchy. An MSW resonance is predicted to occur in multi-GeV, upward-going atmospheric neutrinos, which travel through Earth's mantle [11]. MINOS is the first experiment to probe this resonance by measuring ν_μ and $\bar{\nu}_\mu$ interactions separately with atmospheric neutrinos, yielding sensitivity to the mass hierarchy and θ_{23} octant.

MINOS [12] has previously reported measurements of ν_e and $\bar{\nu}_e$ appearance in accelerator ν_μ and $\bar{\nu}_\mu$ beams. Measurements of $\nu_\mu \to \nu_e$ appearance in accelerator neutrinos have also been published by T2K [13]. Both results are based on three-flavor analyses. For accelerator neutrinos, the $\nu_\mu \to \nu_e$ appearance probability in matter, expanded to second order in $\alpha \equiv \Delta m_{21}^2 / \Delta m_{31}^2$ (≈ 0.03), is given by [14]:

$$P(\nu_\mu \to \nu_e) \approx \sin^2\theta_{23}\sin^2 2\theta_{13}\frac{\sin^2\Delta(1-A)}{(1-A)^2}$$

$$+ \alpha\tilde{J}\cos(\Delta \pm \delta_{CP})\frac{\sin\Delta A}{A}\frac{\sin\Delta(1-A)}{(1-A)}$$

$$+ \alpha^2\cos^2\theta_{23}\sin^2 2\theta_{12}\frac{\sin^2\Delta A}{A^2}. \quad (4)$$

In this expression, $\tilde{J} \equiv \cos\theta_{13}\sin 2\theta_{13}\sin 2\theta_{12}\sin 2\theta_{23}$, $\Delta \equiv \Delta m_{31}^2 L_\nu/4E_\nu$ and the plus (minus) sign applies to neutrinos (antineutrinos). The first term in Eq. (4) is proportional to $\sin^2\theta_{23}$ and breaks the θ_{23} octant degeneracy. In addition, the dependence on A is sensitive to the mass hierarchy and the second term in the expansion is sensitive to CP violation. In this Letter, we strengthen the constraints on δ_{CP}, the θ_{23} octant, and the mass hierarchy obtained from the MINOS appearance data [12] by combining the complete MINOS disappearance and appearance data and by exploiting the improved precision on θ_{13} from reactor experiments.

In the MINOS experiment, the accelerator neutrinos are produced by the NuMI facility [15], located at the Fermi National Accelerator Laboratory. The complete MINOS accelerator neutrino data set comprises exposures of 10.71×10^{20} protons on target using a ν_μ-dominated beam and 3.36×10^{20} protons on target using a $\bar{\nu}_\mu$-enhanced beam [7]. These data were acquired in the "low energy" NuMI beam configuration [15], where the neutrino event energy peaks at 3 GeV. The spectrum and composition of the beam are measured using two steel-scintillator tracking detectors with toroidal magnetic fields. The Near and Far detectors are located 1.04 and 735 km downstream of the production target, respectively. The 5.4 kton Far Detector is installed 705 m (2070 m water equivalent) underground in the Soudan Underground Laboratory and is equipped with a scintillator veto shield for rejection of cosmic-ray muons. These features have enabled MINOS to collect 37.88 kton-y of atmospheric neutrino data [16].

The oscillation analysis uses charged-current (CC) interactions of both muon and electron neutrinos. These events are distinguished from neutral-current (NC) backgrounds by the presence of a muon track or electromagnetic shower, respectively. The events also typically contain shower activity from the hadronic recoil system. The selection of accelerator ν_μ CC and $\bar{\nu}_\mu$ CC events is based on a multivariate k-nearest-neighbor classification algorithm using a set of input variables characterizing the topology and energy deposition of muon tracks [17]. The selected events are separated into contained-vertex neutrinos, with reconstructed interaction positions inside the fiducial volume of the detectors, and non-fiducial muons, in which the neutrino interactions occur outside the fiducial volume or in the surrounding rock. The contained-vertex events are further divided into candidate ν_μ and $\bar{\nu}_\mu$ interactions based on the curvature of their muon tracks. In the oscillation fit, the events are binned as a function of reconstructed neutrino energy. For contained-vertex events, this is taken as the sum of the muon and hadronic shower energy measurements; for nonfiducial muons, the muon energy alone is used as the neutrino energy estimator. To improve the sensitivity to oscillations, the contained-vertex ν_μ events from the ν_μ-dominated beam are also binned according to their calculated energy resolution [18–20]. The predicted energy spectra in the Far Detector are derived from the observed data in the Near Detector using a beam transfer matrix [21].

The selection of accelerator ν_e CC and $\bar{\nu}_e$ CC events is based on a library-event-matching algorithm that performs hit-by-hit comparisons of contained-vertex shower-like events with a large library of simulated neutrino interactions [22–24]. The events are required to have reconstructed energies in the range 1–8 GeV, where most of the ν_e and $\bar{\nu}_e$ appearance is predicted to occur. The 50 best-matching events from the library are used to calculate a set of classification variables that are combined into a single discriminant using an artificial neural network. The selection does not discriminate between ν_e and $\bar{\nu}_e$ interactions. The selected events are binned as a function of the reconstructed energy and library-event-matching discriminant. The background contributions from NC, ν_μ CC, and $\bar{\nu}_\mu$ CC interactions, and intrinsic ν_e CC and $\bar{\nu}_e$ CC interactions from the beam, are determined using samples of Near Detector data collected in different beam configurations. The backgrounds in the Far Detector are calculated from these Near Detector components [25]. The rates of appearance in the Far Detector are derived from the ν_μ CC and $\bar{\nu}_\mu$ CC spectra measured in the Near Detector [12].

Atmospheric neutrinos are separated from the cosmic-ray muon background using selection criteria that identify either a contained-vertex interaction or an upward-going or horizontal muon track [26,27]. For contained-vertex events, the background is further reduced by checking for associated energy deposits in the veto shield. The event selection yields samples of contained-vertex and nonfiducial muons, which are each separated into candidate ν_μ CC and $\bar{\nu}_\mu$ CC interactions. These samples of muons are binned as a function of $\log_{10}(E)$ and $\cos\theta_z$, where E is the reconstructed energy of the event in GeV and θ_z is the zenith angle of the muon track. This two-dimensional binning scheme enhances the sensitivity to the MSW resonance. The results remain in close agreement with the two-flavor analysis of ν_μ and $\bar{\nu}_\mu$ disappearance, in which these data were binned as a function of $\log_{10}(L/E)$ [7]. A sample of contained-vertex showers is also selected from the data, composed mainly of NC, ν_e CC, and $\bar{\nu}_e$ CC interactions. These events are grouped into a single bin, since they have negligible sensitivity to oscillations but constrain the overall flux normalization. The predicted event rates in each selected sample are calculated from a Monte Carlo simulation of atmospheric neutrino interactions in the Far Detector [16,28]. The cosmic-ray muon backgrounds are obtained from the observed data by reweighting the events tagged by the veto shield according to the measured shield inefficiency [26].
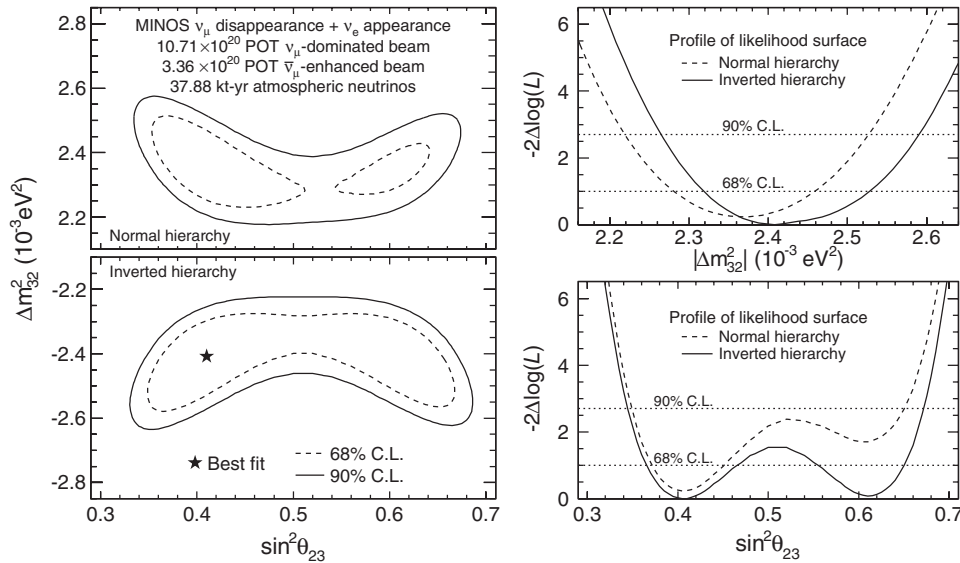
FIG. 1.　The left panels show the 68% and 90% confidence limits on Δm^2_{32} and $\sin^2 \theta_{23}$ for the normal hierarchy (top) and inverted hierarchy (bottom). At each point in this parameter space, the likelihood function is maximized with respect to $\sin^2 \theta_{13}$, δ_{CP} and all of the systematic parameters. The $-2\Delta \log(\mathcal{L})$ surface is calculated relative to the overall best fit, which is indicated by the star. The right panels show the 1D likelihood profiles as a function of Δm^2_{32} and $\sin^2 \theta_{23}$ for each hierarchy. The horizontal dotted lines indicate the 68% and 90% C.L.

For all the data samples, the predicted event spectra in the Far Detector are reweighted to account for oscillations, and the backgrounds from ν_τ and $\bar{\nu}_\tau$ appearance are included. The oscillation probabilities are calculated directly from the PMNS matrix using algorithms optimized for computational efficiency [29]. The probabilities account for the propagation of neutrinos through Earth. For accelerator neutrinos, a constant electron density of $1.36 \, \mathrm{mol \, cm^{-3}}$ is assumed. For atmospheric neutrinos, Earth is modeled by four layers of constant electron density: an inner core ($r < 1220$ km, $n_e = 6.05 \, \mathrm{mol \, cm^{-3}}$); an outer core ($1220 < r < 3470$ km, $n_e = 5.15 \, \mathrm{mol \, cm^{-3}}$); the mantle ($3470 < r < 6336$ km, $n_e = 2.25 \, \mathrm{mol \, cm^{-3}}$); and the crust ($r > 6336$ km, $n_e = 1.45 \, \mathrm{mol \, cm^{-3}}$). This four-layer approximation reflects the principal structures of the PREM model [30]. Comparisons with a more detailed 42-layer model yield similar oscillation results.

The oscillation parameters are determined by applying a maximum likelihood fit to the data. The parameters Δm^2_{32}, $\sin^2 \theta_{23}$, $\sin^2 \theta_{13}$ and δ_{CP} are varied in the fit. The

mixing angle θ_{13} is subject to an external constraint of $\sin^2 \theta_{13} = 0.0242 \pm 0.0025$, based on a weighted average of the published results from the Daya Bay [31], RENO [4], and Double Chooz [5] reactor experiments. This constraint is incorporated into the fit by adding a Gaussian penalty term to the likelihood function. The fit uses fixed values of $\Delta m^2_{21} = 7.54 \times 10^{-5} \, \mathrm{eV^2}$ and $\sin^2 \theta_{12} = 0.307$ [32]. The impact of these two parameters is evaluated by shifting them in the fit according to their uncertainties; the resulting shifts in the fitted values of Δm^2_{32} and $\sin^2 \theta_{23}$ are found to be negligibly small. The likelihood function contains 32 nuisance parameters, with accompanying penalty terms, that account for the major systematic uncertainties in the simulation of the data [16,23,33]. The fit proceeds by summing the separate likelihood contributions from the ν_μ disappearance [7] and ν_e appearance [12] data sets, taking their systematic parameters to be uncorrelated.

Figure 1 shows the 2D confidence limits on Δm^2_{32} and $\sin^2 \theta_{23}$, obtained by maximizing the likelihood function at each point in this parameter space with respect to $\sin^2 \theta_{13}$,

TABLE I.　The best-fit oscillation parameters obtained from this analysis for each combination of mass hierarchy and θ_{23} octant. Also listed are the $-2\Delta \log(\mathcal{L})$ values for each of the four combinations, calculated relative to the overall best-fit point.

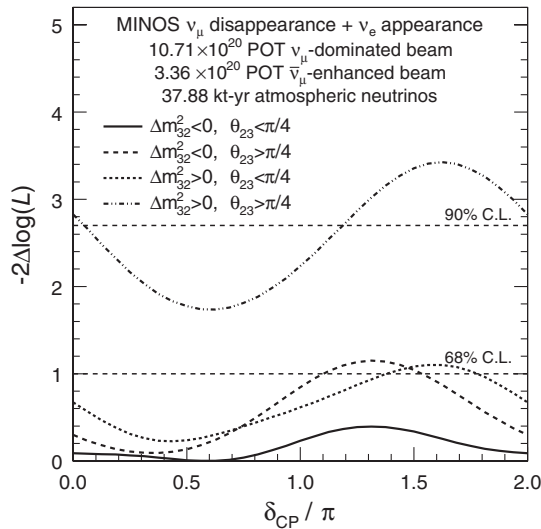| Mass hierarchy	θ_{23} octant	$\Delta m^2_{32}/10^{-3} \, \mathrm{eV^2}$	$\sin^2 \theta_{23}$	$\sin^2 \theta_{13}$	δ_{CP}/π	$-2\Delta \log(\mathcal{L})$
$\Delta m^2_{32} < 0$	$\theta_{23} < \pi/4$	-2.41	0.41	0.0243	0.62	0
$\Delta m^2_{32} < 0$	$\theta_{23} > \pi/4$	-2.41	0.61	0.0241	0.37	0.09
$\Delta m^2_{32} > 0$	$\theta_{23} < \pi/4$	$+2.37$	0.41	0.0242	0.44	0.23
$\Delta m^2_{32} > 0$	$\theta_{23} > \pi/4$	$+2.35$	0.61	0.0238	0.62	1.74

FIG. 2.   The 1D likelihood profile as a function of δ_{CP} for each combination of mass hierarchy and θ_{23} octant. For each value of δ_{CP}, the likelihood function is maximized with respect to $\sin^2\theta_{13}$, $\sin^2\theta_{23}$, Δm_{32}^2, and all of the systematic parameters. The horizontal dashed lines indicate the 68% and 90% confidence limits.

δ_{CP}, and all of the systematic parameters. Also shown are the corresponding 1D likelihood profiles as a function of Δm_{32}^2 and $\sin^2\theta_{23}$. The 68% (90%) confidence limits on these parameters are calculated by taking the range of negative log-likelihood values with $-2\Delta\log(\mathcal{L}) < 1.00$ (2.71) relative to the overall best fit. This yields $|\Delta m_{32}^2| = [2.28\text{--}2.46] \times 10^{-3}$ eV^2 (68% C.L.) and $\sin^2\theta_{23} = 0.35\text{--}0.65$ (90% C.L.) in the normal hierarchy, and $|\Delta m_{32}^2| = [2.32\text{--}2.53] \times 10^{-3}$ eV^2 (68% C.L.) and $\sin^2\theta_{23} = 0.34\text{--}0.67$ (90% C.L.) in the inverted hierarchy. The data disfavor maximal mixing ($\theta_{23} = \pi/4$) by $-2\Delta\log(\mathcal{L}) = 1.54$. The measurements of Δm_{32}^2 are the most precise that have been reported to date.

The data also constrain δ_{CP}, the θ_{23} octant degeneracy and the mass hierarchy. Table I lists the best-fit oscillation parameters for each combination of octant and mass hierarchy, and the differences in negative log-likelihood relative to the overall best fit. Assuming $\theta_{23} > \pi/4$ ($\theta_{23} < \pi/4$), the data prefer the inverted hierarchy by $-2\Delta\log(\mathcal{L}) = 1.65(0.23)$. The combination of normal hierarchy and higher octant is disfavored by 1.74 units of $-2\Delta\log(\mathcal{L})$, strengthening the previous constraints from ν_e and $\bar{\nu}_e$ appearance [12]. Figure 2 shows the 1D likelihood profile as a function of δ_{CP} for each of the four possible combinations. The data disfavor 36% (11%) of the parameter space defined by δ_{CP}, the θ_{23} octant, and the mass hierarchy at 68% (90%) C.L.

In summary, we have presented the first combined analysis of ν_μ disappearance and ν_e appearance data by a long-baseline neutrino experiment. The results are based on the complete set of MINOS accelerator and atmospheric neutrino data. A combined analysis of these data sets yields precision measurements of Δm_{32}^2 and $\sin^2\theta_{23}$, along with

new constraints on the three-parameter space defined by δ_{CP}, the θ_{23} octant, and the mass hierarchy.

---

[*]Deceased.
[1] Z. Maki, M. Nakagawa, and S. Sakata, Prog. Theor. Phys. **28**, 870 (1962); B. Pontecorvo, Sov. Phys. JETP **26**, 984 (1968); V. N. Gribov and B. Pontecorvo, Phys. Lett. **28B**, 493 (1969).
[2] J. Beringer et al. (Particle Data Group), Phys. Rev. D **86**, 010001 (2012).
[3] F. An et al. (Daya Bay Collaboration), Phys. Rev. Lett. **112**, 061801 (2014).
[4] J. K. Ahn et al. (RENO Collaboration), Phys. Rev. Lett. **108**, 191802 (2012).
[5] Y. Abe et al. (Double Chooz Collaboration), Phys. Rev. D **86**, 052008 (2012).
[6] D. G. Michael et al. (MINOS Collaboration), Nucl. Instrum. Methods Phys. Res., Sect. A **596**, 190 (2008).
[7] P. Adamson et al. (MINOS Collaboration), Phys. Rev. Lett. **110**, 251801 (2013).
[8] H. Nunokawa, S. Parke, and R. Zukanovich Funchal, Phys. Rev. D **72**, 013009 (2005).
[9] L. Wolfenstein, Phys. Rev. D **17**, 2369 (1978); S. P. Mikheev and A. Y. Smirnov, Sov. J. Nucl. Phys. **42**, 913 (1985).
[10] C. Giunti, C. W. Kim, and M. Monteno, Nucl. Phys. **B521**, 3 (1998).
[11] S. Palomares-Ruiz and S. T. Petcov, Nucl. Phys. **B712**, 392 (2005).
[12] P. Adamson et al. (MINOS Collaboration), Phys. Rev. Lett. **110**, 171801 (2013).
[13] K. Abe et al. (T2K Collaboration), Phys. Rev. Lett. **112**, 061802 (2014).
[14] A. Cervera, A. Donini, M. B. Gavela, J. J. Gomez Cádenas, P. Hernández, O. Mena, and S. Rigolin, Nucl. Phys. **B579**, 17 (2000).
[15] K. Anderson et al., Report No. FERMILAB-DESIGN-1998-01 (1998).
[16] P. Adamson et al. (MINOS Collaboration), Phys. Rev. D **86**, 052007 (2012).
[17] R. Ospanov, Ph.D. thesis, University of Texas at Austin, 2008.
[18] J. Mitchell, Ph.D. thesis, University of Cambridge, 2011.
[19] S. J. Coleman, Ph.D. thesis, College of William & Mary, 2011.
[20] C. J. Backhouse, D.Phil. thesis, University of Oxford, 2011.
[21] P. Adamson et al. (MINOS Collaboration), Phys. Rev. D **77**, 072002 (2008).
[22] J. P. Ochoa Ricoux, Ph.D. thesis, California Institute of Technology, 2009.

[23] R. B. Toner, Ph.D. thesis, University of Cambridge, 2011.
[24] A. P. Schreckenberger, Ph. D. thesis, University of Minnesota, 2013.
[25] J. A. B. Coelho, Ph.D. thesis, Universidade Estadual de Campinas, 2012.
[26] J. D. Chapman, Ph.D. thesis, University of Cambridge, 2007.
[27] B. P. Speakman, Ph.D. thesis, University of Minnesota, 2007.
[28] G. D. Barr, T. K. Gaisser, P. Lipari, S. Robbins, and T. Stanev, Phys. Rev. D **70**, 023006 (2004).
[29] J. Kopp, Int. J. Mod. Phys. C **19**, 523 (2008).
[30] A. M. Dziewonski and D. L. Anderson, Phys. Earth Planet. Interiors **25**, 297 (1981).
[31] F. P. An *et al.* (Daya Bay Collaboration), Chin. Phys. C **37**, 011001 (2013).
[32] G. L. Fogli, E. Lisi, A. Marrone, D. Montanino, A. Palazzo, and A. M. Rotunno, Phys. Rev. D **86**, 013012 (2012).
[33] P. Adamson *et al.* (MINOS Collaboration), Phys. Rev. Lett. **106**, 181801 (2011).